Title
Preservation and detectability of shock-induced magnetization

Authors
Tikoo, Sonia M
Gattacceca, Jérôme
Swanson-Hysell, Nicholas L
et al.

Publication Date
2015-07-29

DOI
10.1002/2015JE004840

Peer reviewed

Preservation and detectability of shock-induced magnetization

Sonia M. Tikoo[1,2], Jérôme Gattacceca[3,4], Nicholas L. Swanson-Hysell[1], Benjamin P. Weiss[1,4], Clément Suavet[4], and Cécile Cournède[3]

[1]Department of Earth and Planetary Science, University of California, Berkeley, CA 94720, USA.

[2]Berkeley Geochronology Center, 2455 Ridge Road, Berkeley, CA 94709, USA.

[3]CNRS, Aix-Marseille University, CEREGE UM34, Aix-en-Provence, France.

[4]Department of Earth, Atmospheric, and Planetary Sciences, Massachusetts Institute of Technology (MIT), 77 Massachusetts Avenue, Cambridge, MA 02139, USA.

Final version for publication in Journal of Geophysical Research - Planets
Accepted 07/24/2015
DOI:10.1002/2015JE004840

Abstract

An understanding of the effects of hypervelocity impacts on the magnetization of natural samples is required for interpreting paleomagnetic records of meteorites, lunar rocks, and cratered planetary surfaces. Rocks containing ferromagnetic minerals have been shown to acquire shock remanent magnetization (SRM) due to the passage of a shock wave in the presence of an ambient magnetic field. In this study, we conducted pressure remanent magnetization (PRM) acquisition experiments on a variety of natural samples as an analog for SRM acquisition at pressures ranging up to 1.8 GPa. Comparison of the alternating field (AF) and thermal demagnetization behavior of PRM confirms that AF demagnetization is a more efficient method for removing SRM overprints than thermal demagnetization because SRM may persist to unblocking temperatures approaching the Curie temperatures of magnetic minerals. The blocking of SRM to high temperatures suggests that SRM could persist without being eradicated by viscous relaxation over geologic timescales. However, SRM has been rarely observed in natural samples likely because of two factors: [1] other forms of impact-related remanence (e.g., thermal remanent magnetization from impact-related heating or chemical remanent magnetization from post-impact hydrothermal activity) are often acquired by target rocks that overprint SRM, and [2] low SRM acquisition efficiencies may prevent SRM from being distinguished from the underlying primary remanence or other overprints due to its low magnetization intensity.

1. Introduction

The ubiquity of hypervelocity impact events throughout solar system history motivates an understanding of the effects of impacts on both terrestrial and extraterrestrial rocks. In the context of paleomagnetism, shock remagnetization is expected to occur in any geologic environment that has been subjected to impacts. Shock remanent magnetization (SRM) may be acquired nearly instantaneously as the shock wave from an impact passes through a rock in the presence of a magnetic field [*Nagata*, 1971; *Pohl et al.*, 1975]. SRM is usually aligned with the ambient magnetizing field with an intensity proportional to the field strength for weak planetary fields (~1-2500 μT) [*Nagata*, 1971; *Gattacceca et al.*, 2008; *Gattacceca et al.*, 2010a]. Therefore, SRM is capable of recording long-lived core dynamo magnetic fields as well as transient fields such as those hypothesized to be generated or amplified by impact plasmas [*Srnka*, 1977; *Crawford and Schultz*, 1993; *Hood and Artemieva*, 2008]. SRM has been proposed as a potential source for the natural remanent magnetization (NRM) present in some lunar samples [*Cisowski et al.*, 1976; *Gattacceca et al.*, 2010b] and meteorites [*Weiss et al.*, 2010] as well as for secondary magnetization components present in rocks from terrestrial impact craters (e.g., *Halls* [1979]). In the absence of an ambient field, shock waves can demagnetize rocks [*Nagata*, 1971; *Gattacceca et al.*, 2006]. Shock demagnetization may be responsible for the modification of magnetic anomalies observed in the Martian [*Hood et al.*, 2003] and lunar crust [*Halekas et al.*, 2002].

SRM may be acquired in multiple ways that depend on the nature of the ferromagnetic grains within a rock. Shock waves remagnetize multidomain (MD) grains through the rearrangement of domain walls [*Bogdanov and Vlasov*, 1966; *Nagata*, 1973]. In single domain (SD) grains, shock-induced stresses introduce magnetoelastic energy that can exceed the anisotropy energy associated with a pre-existing remanent magnetization and impart a new magnetization [*Hodych*, 1977; *Dunlop and Ozdemir*, 1997]. Shock pressures in excess of the Hugoniot elastic limit (typically ~3 GPa for silicates) may introduce crystallographic defects that result in irreversible changes to intrinsic magnetic properties and can impart magnetic anisotropy [*Gattacceca et al.*, 2007; *Louzada et al.*, 2007; *Gilder and Le Goff*, 2008; *Mang et al.*, 2013]. As rocks experience decompression, these effects combine to impart rocks with SRM or its hydrostatic analog, pressure remanent magnetization (PRM). Note that in the literature another term, piezoremanent magnetization (also abbreviated as PRM; e.g., *Nagata and Carleton* [1968] and *Gattacceca et al.* [2010a]), has been inconsistently used to describe remanence induced through either hydrostatic or non-hydrostatic pressure. The mechanism of PRM acquisition may differ somewhat from that of SRM for at least two reasons. First, only weak deviatoric stresses are present when rocks are pressurized quasi-hydrostatically in the laboratory [*Nagata*, 1966; *Martin and Noel*, 1988]. Second, the pressurization time in typical PRM experiments (>10 s) is longer than the duration of laser shock (~10^{-9} to 10^{-8} s) or typical natural impact events (~10^{-3} to 1 s) that would impart SRM. Nevertheless, we consider PRM to be a good analog for SRM, at least for peak pressures <~2 GPa. Similar behavior between PRM and SRM at these pressures has been observed in acquisition experiments on some lunar rocks and the Allende meteorite that have shown that these samples acquire similar intensities of PRM and SRM at equivalent pressures [*Nagata*, 1971; *Gattacceca et al.*, 2010b; *Carporzen et al.*, 2011]. Pressure experiments on natural pyrrhotite also indicate that variations in non-hydrostaticity do not significantly affect magnetization intensity and other magnetic properties at these pressures [*Gilder et al.*, 2011].

The acquisition of SRM and PRM and the response of these remanences to alternating field (AF) demagnetization have been described in several studies [*Gattacceca et al.*, 2007; *Gattacceca et al.*, 2008; *Gattacceca et al.*, 2010a]. PRM and SRM are recorded preferentially in the low coercivity fraction of magnetic grains and can therefore be removed more efficiently using progressive AF demagnetization than other forms of remanence such as thermoremanent magnetization (TRM), anhysteretic remanent magnetization (ARM, often used as a room-temperature analog for TRM), and saturation isothermal remanent magnetization (SIRM). In contrast, the thermal demagnetization behaviors of SRM and PRM have not yet been studied in detail, with the exception of some preliminary analyses of FeNi-bearing lunar materials [*Cisowski et al.*, 1973; *Gattacceca et al.*, 2010b].

Because nearly all meteorites and rocks from cratered planetary surfaces (including the lunar samples from the Apollo missions) have experienced some level of shock, it is important to understand the effects of shock on remanent magnetization, especially at relatively low pressures where petrographic evidence of shock may not be observed (<5 GPa [*Stoffler et al.*, 2006]). The magnetization of rocks submitted to pressures <2 GPa is of particular interest because the volume of target rocks shocked to <2 GPa during hypervelocity impacts is ~2-3 times the volume of target rocks shocked to pressures >2 GPa (estimated from *Robertson and Grieve* [1977] and *Louzada and Stewart* [2009]). In this study, we determine the relative intensities of PRM acquired at pressures <2 GPa compared to TRM for samples representing a wider range of rock types and ferromagnetic mineralogies than previously studied. In addition, we investigate the thermal demagnetization properties of PRM and compare them to those of other remanences. We utilize our results to assess the paleomagnetic stability of PRM and SRM over geologic timescales and to provide a framework for identifying SRM in natural samples.

2. Samples and Methods

2.1. Samples and handling

We analyzed the PRM properties of a variety of terrestrial and extraterrestrial samples with different magnetic mineralogies and rock magnetic properties including FeNi alloys, magnetite, pyrrhotite, titanomagnetite, and combinations of these ferromagnetic minerals (Table 1). Our terrestrial samples include a titanomagnetite-bearing Pleistocene basalt (BB) from Chanteuges, Haute-Loire, France and a magnetite-bearing microdiorite (EE) from the Esterel range, France, whose rock magnetic properties were previously characterized by *Gattacceca et al.* [2007; 2008]. We also studied a Mesoproterozoic titanomagnetite-bearing diabase (DeI3-6) collected from a dike associated with the Osler Volcanic Group [*Swanson-Hysell et al.*, 2014] within the Slate Islands impact crater, Canada. Numerous extraterrestrial samples were also analyzed. Our magnetite- and pyrrhotite-bearing samples include the Martian meteorite Tissint [*Gattacceca et al.*, 2013], the CV3 carbonaceous chondrite Allende (e.g., Carporzen et al. [2011]), the Rumuruti-like (R) chondrite PCA 91002, and the CM carbonaceous chondrites Cold Bokkeveld, Mighei, Murchison, Murray, Nogoya, and Paris [*Cournede et al.*, 2015]. We also analyzed the FeNi-bearing mare basalts 15556 [*Tikoo et al.*, 2012], 12022 [*Tikoo et al.*, 2014], 10020 [*Shea et al.*, 2012], 10017 and 10049 [*Suavet et al.*, 2013], ordinary chondrites NWA 6490 and NWA 7621, and basaltic eucrite ALHA81001 [*Fu et al.*, 2012]. Finally, we studied the magnetite-bearing CV3 chondrite Kaba and the pyrrhotite-bearing R chondrite LAP 03639. Sample handling, PRM acquisition experiments, and rock magnetic experiments were conducted within magnetically shielded rooms (ambient DC field < 250 nT) in paleomagnetism laboratories at the Massachusetts Institute of Technology (MIT), CEREGE (Aix-en-Provence, France), and the University of California, Berkeley.

2.2. PRM acquisition

Specimens ranging in mass from 30-350 mg were imparted with a PRM using a nearly nonmagnetic pressure cell in the presence of a controlled laboratory field [*Gattacceca et al.*, 2010b]. Prior to PRM acquisition, the samples were demagnetized using AF or thermal demagnetization. We were able to fully demagnetize (i.e., residual magnetization was <95% of the original NRM) all samples except for LAP 03639 (residual was ~15% of the original NRM) and DeI3-6 (which acquired spurious gyroremanent magnetization during AF demagnetization with intensity ~10% of the original NRM). Any residual magnetizations present were removed from the PRM data by vector subtraction. Following demagnetization pre-treatment, specimens were placed in an 8 mm × 20 mm Teflon capsule and submerged in polyethylsiloxane fluid. The capsule was then placed in a nearly nonmagnetic piston-cylinder pressure cell made of the alloy $Ni_{57}Cr_{40}Al_3$ [*Sadykov*, 2008]. The cell has a magnetic moment of 2×10^{-8} Am^2 and is designed to allow hydrostatic loading up to 1.8 GPa. A solenoidal coil wrapped around the pressure cell was used to produce a dc magnetic field oriented along the long axis of the cell. Field intensities were calibrated using a Hall probe. A known magnetic field (500 µT, 750 µT, or 800 µT) was applied to the cell. The cell was then loaded with pressures ranging between 0.18 and 1.8 GPa using a Specac 15-ton manual hydraulic press. Specimens were held at pressure for ~1 minute and then the load was released in the presence of the applied magnetic field.

2.3. Magnetic analyses

Following PRM acquisition, we measured the acquired magnetization and then demagnetized specimens using either stepwise AF or thermal methods. To compare the demagnetization behavior of PRM to that of other forms of remanence, additional specimens from each parent rock sample (subjected to the same pre-treatment as the PRM specimen) were given TRM, ARM, and/or SIRM. ARM was applied with a 0.1 mT dc bias field and a 290-300 mT ac field. SIRM was applied in a pulse field of 900 mT for FeNi and magnetite-bearing samples and a 3 T field for pyrrhotite-bearing samples. Measurements of magnetization, progressive demagnetization, and rock magnetic experiments were carried out using 2G Enterprises Superconducting Rock Magnetometers at MIT, CEREGE, or UC Berkeley. The MIT and UC Berkeley magnetometers are equipped with automated sample handling and AF demagnetization equipment [*Kirschvink et al.*, 2008]. Thermal demagnetization was conducted in ASC Scientific ovens with residual magnetic fields <5 nT. Nearly all thermally demagnetized samples were given an AF pre-treatment of 1.5 mT prior to thermal demagnetization to remove any weak isothermal remanent magnetization (IRM) that may have been acquired from the pressure cell solenoid (500-800 μT dc field). Two exceptions to this protocol were made for the ordinary chondrites NWA 6490 and NWA 7629 due to their exceptionally low coercivities (they lose ~40% of ARM by AF 1.5 mT). FeNi-bearing samples were thermally demagnetized in a controlled oxygen fugacity atmosphere using a calibrated H_2-CO_2 mixture at MIT to avoid alteration of the magnetic carriers [*Suavet et al.*, 2014]. Hysteresis properties were measured on Princeton Instruments vibrating sample magnetometers at CEREGE and the Institute for Rock Magnetism at the University of Minnesota.

3. Results

3.1. PRM acquisition

We define PRM acquisition efficiency (α) as the ratio of PRM to TRM acquired in the same ambient field. One of the goals of our study was to determine how α varies as a function of ferromagnetic mineralogy, domain state, and pressure. Observations from a wide range of samples and ferromagnetic mineralogies suggest the following generalized relationship between TRM and SIRM:

$$\mathrm{TRM} \approx \frac{\mathrm{SIRM} \cdot B}{3000\ \mu\mathrm{T}} \quad (1)$$

where B is the strength of the ambient field in μT [*Kletetschka et al.*, 2003; *Gattacceca and Rochette*, 2004]. Numerous studies indicate that this relationship is generally accurate to within a factor of ~2-3 [e.g., *Kletetschka et al.*, 2003; *Gattacceca and Rochette*, 2004; *Tikoo et al.*, 2014; *Weiss and Tikoo*, 2014]. To avoid thermochemical alteration from heating, we did not impart the PRM specimens with laboratory TRM. Instead, we used equation (1) and PRM intensities from our acquisition experiments to estimate α (i.e., PRM/TRM) for all samples. We normalized PRM efficiency data from after AF demagnetization to 2 mT ($\alpha_{2\ \mathrm{mT}}$) to remove any viscous contributions imparted by the pressure cell solenoid from the PRM data. In a natural setting, SRM or PRM acquired by such a low-coercivity (<2 mT) fraction of ferromagnetic grains would likely be eradicated by other secondary processes such as the acquisition of viscous remanent magnetization (VRM). Therefore, we do not anticipate that our overall conclusions regarding PRM and SRM efficiency in nature would change substantially by the exclusion of PRM data at these lowest AF levels.

PRM acquisition efficiency ($\alpha_{2\ \mathrm{mT}}$) generally increased with peak pressure for all samples. However, we observed that different samples had vastly different efficiencies for the same pressure level, ranging between negligible PRM acquisition for ALHA81001 ($\alpha_{2\ \mathrm{mT}} = 5\times10^{-5}$) to substantial PRM acquisition for EE ($\alpha_{2\ \mathrm{mT}} = 0.22$) at a peak pressure of 1.8 GPa (Fig. 1). We observed that samples with lower remanent coercivities (B_{cr}) typically had higher $\alpha_{2\ \mathrm{mT}}$ values than samples with lower B_{cr} values (Fig. 2), consistent with the observation that PRM is preferentially acquired by low coercivity grains. Considering $\alpha_{2\ \mathrm{mT}}$ values in conjunction with the hysteresis data suggests that rocks with larger populations of MD grains have higher PRM efficiencies, at least for samples containing a single ferromagnetic mineralogy (e.g., only magnetite or only FeNi) (Fig. 3). For example, the magnetite-bearing microdiorite EE and titanomagnetite-bearing basalt BB have higher PRM efficiencies than the more SD-like (i.e., having higher M_{rs}/M_s and lower B_{cr}/B_c) samples DeI3-6 and Kaba (Figs. 2 and 3). Similarly, among FeNi-bearing samples, the MD lunar basalts and ordinary chondrite NWA 6490 have higher PRM efficiencies than the more SD-like eucrite ALHA81001. However, this relationship between PRM efficiency and domain state is difficult to determine when comparing samples with more than one magnetic carrier mineral (such as rocks with both magnetite and pyrrhotite). In such cases, differences in both PRM efficiency and bulk hysteresis properties may be associated with variations in the relative concentrations of each ferromagnetic mineral present between samples (Section 4.3).

3.2. AF demagnetization of PRM

We conducted AF demagnetization experiments of laboratory PRM acquired at a range of pressures ≤1.8 GPa on at least one specimen from each rock studied. Consistent with previous experiments focused on SRM demagnetization behavior [*Gattacceca et al.*, 2007; *Gattacceca et al.*, 2008; *Gattacceca et al.*, 2010a], we found that PRM was confined to lower AF levels (<20-50 mT, depending on the sample) than SIRM, TRM, and ARM. The median destructive field (MDF: the AF amplitude required to remove half of a remanence) of PRM increased with applied pressure, but always remained lower than those of TRM, ARM, and SIRM at the pressures studied (Fig. 4). The AF levels necessary to remove the laboratory-induced remanences were correlated with the domain states of the samples. For example, PRM was removed more efficiently from the multidomain remanence carriers of the microdiorite sample EE than from the remanence carriers of diabase sample DeI3-6, which have rock magnetic behavior characteristic of pseudo-single domain grains, even though low-titanium magnetite is the primary magnetic carrier for both samples. Therefore, our PRM acquisition and AF demagnetization results both suggest that PRM is preferentially acquired by low coercivity, multidomain grains.

3.3. Thermal demagnetization of PRM

We conducted thermal demagnetization of PRM on selected specimens representing each group of ferromagnetic mineralogies. We found that for all samples, PRM persisted to unblocking temperatures approaching the Curie temperatures (or at least the maximum unblocking temperatures of SIRM) of the ferromagnetic minerals (Fig. 5). For example, the magnetite-bearing samples did not lose 95% of the PRM overprint until they were heated to temperatures >500 ºC (Fig. 5a, b, c, f). The FeNi-bearing ordinary chondrites NWA 6490 and NWA 7629 lost 95% of their PRM at ~500-550 ºC (Fig. 5d). While this temperature is well below the 780 ºC Curie point of kamacite ($Fe_{0.95-1}Ni_{0-0.05}$), the fact that the SIRM demagnetizes at the same low temperature indicates that these samples either experienced thermochemical alteration during heating or that the remanence carriers in these samples are made of other FeNi alloys with higher Ni contents such as martensite ($Fe_{0.75-0.95}Ni_{0.05-0.25}$) which could demagnetize at similarly low temperatures depending on Ni content [*Swartzendruber et al.*, 1991]. In all cases, PRM (acquired at pressures up to 1.8 GPa) had lower median unblocking temperatures than TRM or ARM although this difference was less pronounced than that seen in the MDF values in the AF demagnetization data. The median unblocking temperatures of PRM generally increased with pressure, but did not exceed those of SIRM, which also had a lower median unblocking temperature than TRM and ARM (Fig. 5).

4. Discussion

4.1. Demagnetization properties of pressure-induced remanence

Although PRM is easily removed at relatively low AF levels compared to other forms of remanence such as full ARM and TRM (Fig. 4), we found that during thermal demagnetization PRM (and SRM) may persist and overlap with higher coercivity magnetizations over nearly the full range of unblocking temperatures in shocked samples (Fig. 6). This result confirms that AF demagnetization methods are more efficient at removing PRM and SRM overprints from rocks than thermal demagnetization. Therefore, if thermal demagnetization is conducted without prior AF pre-treatment, both the primary remanence and any present SRM overprints could be removed simultaneously. Paleomagnetic studies aiming to retrieve paleointensities from Thellier-Thellier style experiments or other thermal methods from the primary (pre-shock) remanence of shocked samples should ideally include an AF pre-treatment prior to thermal demagnetization to ensure that any putative SRM overprints are identified and cleaned from samples properly.

Alternatively, if the goal of a paleomagnetic study is to test whether or not a secondary impact-related remanence is SRM, the distinct AF and thermal demagnetization behavior of SRM (based on its analog, PRM) provides a framework for distinguishing SRM from other forms of remanence such as VRM from long-term exposure to the terrestrial field or thermoviscous remanent magnetization (TVRM) from heating produced in impact settings as a result of significant shock pressures [*Stewart et al.*, 2007]. For relatively high Curie temperature ferromagnetic minerals such as near-stoichiometric magnetite (~580 °C), both VRM and TVRM would likely be removed well below the Curie temperatures during thermal demagnetization in SD and pseudo-single domain (PSD) samples, whereas SRM would persist to higher temperatures. Distinguishing SRM from other remanences may also be challenging for predominantly MD samples because unblocking tail effects could potentially cause all of these forms of remanence to not fully demagnetize until near the Curie temperature [*Xu and Dunlop*, 1994].

4.2. Mechanism(s) behind PRM and SRM acquisition and implications for their paleomagnetic stability

Given the relative ease of removing PRM and SRM using AF demagnetization, the persistence of PRM to relatively high unblocking temperatures during thermal demagnetization experiments requires explanation. In this section, we discuss how this behavior results from the various mechanisms by which PRM and SRM are acquired. Following the treatment of *Dunlop et al.* [1969] for magnetization acquired under uniaxial compression, we first discuss how PRM and SRM may be acquired by and preserved in SD grains according to Néel theory [*Néel*, 1955]. We then discuss the acquisition and preservation of these remanences in MD grains.

4.2.1. Single domain samples

Ferromagnetic grains preferentially retain magnetization along certain directional axes within crystals called easy axes. Grains are remagnetized when the energy barrier preserving an initial magnetization is overcome such that magnetization is re-acquired along a different easy axis or in an antipodal direction along the same axis. The net anisotropy energy of a grain is the sum of the magnetocrystalline, magnetostriction (shape), and magnetoelastic (stress) anisotropy energies [*Dunlop and Ozdemir*, 1997]. Several changes in magnetic anisotropy have been observed to occur when rocks are pressurized:

When ferromagnetic grains are hydrostatically compressed, the constants of magnetocrystalline anisotropy (K_1 and K_2 for a cubic crystal structure) have been observed to decrease with increasing pressure while the magnetostriction constants (λ_{100} and λ_{111}) increase with pressure for magnetite [*Nagata and Kinoshita*, 1967]. These constants change at different rates in response to pressure (K_1 and K_2 decrease less rapidly than λ_{100} and λ_{111} increase with pressure) [*Nagata and Kinoshita*, 1967]. Therefore, even though there is no preferred compression axis, the resulting change in total anisotropy can lead to remagnetization.

Uniaxial compression experiments demonstrate that remanence anisotropy and magnetic susceptibility strengthen in the direction perpendicular to a uniaxial compression axis and weaken along the axis parallel to the compression (e.g., *Nagata* [1970] and *Gilder and Le Goff* [2008]). These changes indicate that uniaxial compression introduces stress anisotropy to ferromagnetic grains. As pressure increases, the contribution of stress anisotropy energy increases relative to the magnetocrystalline and shape anisotropy energies (that are simultaneously changing as a result of compression, as discussed in the hydrostatic case above). Considering only shape anisotropy, the total energy for a spheroidal SD grain under a uniaxial stress σ applied parallel to the elongation axis is:

$$E_{tot} = -\mu_0 V \overrightarrow{M_s} \cdot \overrightarrow{H_0} + \frac{1}{2}\mu_0 V M_s \left[(N_b - N_a)M_s - \frac{3\lambda_s \sigma}{\mu_0 M_s}\right] \sin^2\theta \qquad (2)$$

where μ_0 is the permeability of free space, V is the grain volume, $\overrightarrow{M_s}$ is the spontaneous magnetization, $\overrightarrow{H_0}$ represents the applied field, N_a and N_b are the demagnetizing factors when $\overrightarrow{M_s}$ is oriented parallel or perpendicular to the long axis of the grain, λ_s is the magnetostriction (i.e., the magnetization-induced change in shape of a grain), and θ is the angle that $\overrightarrow{M_s}$ is rotated away from the easy axis by $\overrightarrow{H_o}$ (Equation 16.10 of *Dunlop and Ozdemir* [1997]). The expression within the brackets represents the microcoercivity (i.e., the critical field above which the spontaneous magnetization in a grain will undergo an irreversible rotation to another stable orientation).

For shape anisotropy alone, in the absence of pressure, the microcoercivity of a magnetic grain, H_K, is equal to $(N_b - N_a)M_s$. Adding stress parallel to the elongation axis of a spheroidal reduces the microcoercivities of magnetic grains to a new value, $H'_K = H_K - \frac{3\lambda_s\sigma}{\mu_0 M_s}$ (Equation 16.11 of *Dunlop and Ozdemir* [1997]). In contrast, applying uniaxial stress perpendicular to the elongation axis will result in an increase in coercivity. Application of stress at intermediate angles would shift the anisotropy from a uniaxial to a non-uniaxial form. The effect of stress on microcoercivity suggests that imparting SRM may be analogous to imparting IRM in the absence of pressure. During decompression, the bulk anisotropy of a grain will progressively return to its natural (stress-free) state. If an ambient magnetic field is present, the grain will be remagnetized as the spontaneous magnetization aligns itself with the anisotropy easy axis that has the lowest angular deviation from the field direction.

During TRM acquisition, SD grains acquire remanent magnetization as they cool through their respective blocking temperatures. Blocking temperatures vary depending on grain volume and microcoercivity. In contrast, as demonstrated above, acquisition of other forms of remanence such as IRM, PRM, and SRM are principally dependent on coercivity rather than grain volume. The recording of PRM and SRM by coercivity may explain why these remanences are removed more efficiently than TRM by AF demagnetization and also why the thermal demagnetization curves of PRM and IRM qualitatively resemble each other more than they resemble TRM (Fig. 5).

The persistence of PRM and SRM to nearly the Curie temperature during thermal demagnetization experiments likely occurs because the blocking/unblocking temperature distribution in rocks is skewed towards the Curie temperature (see Fig. 8.15 of *Dunlop and Ozdemir* [1997]). The hyperbolic nature of blocking temperature contours demonstrates that large grains with low microcoercivities can have equally high unblocking temperatures as smaller grains with higher coercivities. As such, it is possible for a relatively low coercivity magnetization such as PRM or SRM to persist up to temperatures approaching the Curie temperature.

4.2.2. Pseudo-single domain and multidomain samples

While the theoretical frameworks for characterizing SD remanence and demagnetization properties are well-described, rocks with purely SD magnetic grains are rare in natural settings. PSD and MD grains, which make up the majority of magnetic carriers in most natural samples, do not strictly adhere to the predictions of Néel theory. Rather than by the rotation of spontaneous magnetization (which occurs for SD grains), MD grains magnetize and demagnetize by motions and pinning of domain walls in their interiors. Translation of domain walls requires little energy and can be accomplished in relatively low fields [*Dunlop and Ozdemir,* 1997]. As a result, MD grains are characterized by low coercivities. Our data reveal that samples with low coercivity MD grains have a much higher acquisition efficiency of PRM than samples with a greater concentration of SD grains (Figs. 2,3). This is exemplified by the 3 orders of magnitude difference in $\alpha_{2\,\mathrm{mT}}$ values between the MD ordinary chondrites and lunar samples (~10^{-2}) and that of the eucrite ALHA81001 (~10^{-5}), which has a substantial population of SD grains (Fig. 3). In general, SD grains are unlikely to carry significant amounts of PRM or SRM, at least for the range of pressures explored in this study.

Our results demonstrate that PRM and SRM are dominantly acquired via stress-induced motions of domain walls in MD grains. In PSD and MD grains, PRM may be acquired by the stress-induced nucleation of domain walls [*Boyd et al.*, 1984]. Domain walls stabilize at local energy minima that are often correlated with domain wall pinning localities within the crystal structure [*Muxworthy and Williams,* 2006]. Due to the low coercivity nature of MD grains, domain wall configurations associated with PRM and SRM are easily disrupted by AF demagnetization. This allows PRM and SRM to be removed at relatively low AF levels compared to other forms of remanence such TRM and SIRM, which occupy grains spanning the entire range of coercivities present in a sample. During thermal demagnetization, MD remanence will persist until temperatures are high enough that thermal fluctuations are sufficiently large for domain walls to move to new local energy minima [*Muxworthy and Williams*, 2006]. Another factor that may contribute to the persistence of PRM to high unblocking temperatures is that, in contrast to SD grains, MD grains do not have discrete unblocking temperatures [*Dunlop and Ozdemir*, 2000; 2001]. Laboratory experiments showed that partial TRM (pTRM) imparted to MD magnetite-bearing samples between 370 °C and 350 °C began to demagnetize well below the unblocking temperature predicted by Néel theory, T_B = 350 °C, and that ~90% of the pTRM was not removed until >150 °C above T_B [*Dunlop and Ozdemir*, 2000; 2001]. Indeed, for the largest MD grains, laboratory pTRM was not completely removed until the Curie temperature. For comparison, ~90% of laboratory pTRM imparted to SD samples was removed by temperatures of only ~30 °C above T_B. Therefore, the persistence of PRM and SRM to unblocking temperatures approaching the Curie temperature during thermal demagnetization experiments may also be related to the presence of unblocking tails. In summary, the low coercivity nature of MD grains, coupled with the persistence of some domain wall configurations until elevated temperatures during thermal demagnetization, explains why PRM and SRM are more efficiently removed using AF rather than thermal methods in MD samples.

4.3. Relationships between PRM efficiency and properties of ferromagnetic minerals

In Section 3.1, we demonstrated that for samples containing a single ferromagnetic mineralogy, rocks with larger populations of MD grains have higher PRM efficiencies than more SD-like samples. However, this trend was not as apparent in rocks which contained mixtures of magnetite and pyrrhotite. It is possible that some variability (factor ~2-3) in PRM efficiency values may be attributed to uncertainties in the SIRM normalization calibration constants used to estimate TRM [equation (1)]. However, the primary factor is likely related to the compositions, domain states, grain defect concentrations, and relative abundances of the dominant remanence carriers in a given sample. Among the CM chondrites, magnetic susceptibilities vary by up to ~2 orders of magnitude [*Rochette et al.*, 2008], suggesting the presence of substantial variations in ferromagnetic mineral assemblages, concentrations, and grain sizes even within this one group. Therefore, it is difficult to determine domain states and, in turn, compare PRM efficiency to domain state varabilities that are occurring in multiple phases.

Thermal demagnetization curves of laboratory-induced SIRM may elucidate this issue. For Tissint, ~50% of the initial SIRM remains after the sample is heated above the ~320 °C pyrrhotite Curie temperature (Fig. 2b), whereas only ~10-20% of the initial SIRM remains at the same temperature for all studied CM chondrites (see Fig. 4 of *Cournède et al.* [2015]). The coercivity of magnetite (maximum value ~300 mT) is generally far lower than that of pyrrhotite (maximum value >1 T). Therefore, the higher contribution of (low coercivity) magnetite to the net remanence of Tissint relative to the CM chondrites may explain its higher PRM efficiency.

We also observed that MD FeNi samples had similar PRM efficiencies as PSD magnetite-bearing samples. This raises the possibility that magnetite may have different magnetoelastic properties than FeNi alloys. The Poisson ratios (negative ratio of transverse to axial strain) of these minerals are similar: the mean ratio for magnetite is 0.31 [*Chicot et al.*, 2011], whereas the ratios for metallic Fe and FeNi alloys are ~0.28 [*Ledbetter and Reed*, 1973], suggesting that differences in bulk elastic properties are likely not responsible for differences in PRM efficiency between these minerals. Poisson ratios for pyrrhotite range between ~0.12-0.3 [*Louzada et al.*, 2010], suggesting that pyrrhotite may have a different elastic response to pressure than magnetite and FeNi alloys. However, significant differences do exist between the magnetic anisotropy coefficient values for magnetite and FeNi. For iron at room temperature and atmospheric pressure, the first term of the magnetocrystalline anisotropy constant (K_1) is 4.8×10^4 J/m^3 and the polycrystalline magnetostriction constant at saturation (λ) is -7×10^{-6}. For room-temperature magnetite, $K_1 = -1.35\times10^4$ J/m^3 and $\lambda = 35.8\times10^{-6}$ [*Dunlop and Ozdemir*, 1997]. As discussed in Section 4.2.1, K_1 decreases with pressure while λ increases with pressure. As the total anisotropy of a grain is the sum of its shape, magnetocrystalline, and stress anisotropies, the greater contribution of stress anisotropy relative to magnetocrystallline anisotropy for magnetite (as compared to FeNi) may explain its higher PRM efficiency.

4.4. Identifying SRM in natural samples

While many attempts have been made to identify SRM in natural samples [*Robertson*, 1967; *Halls*, 1979; *Jackson and Van der Voo*, 1986; *Fuller and Cisowski*, 1987; *Iseri et al.*, 1989; *Schmidt and Williams*, 1991; *Pesonen et al.*, 1999; *Carporzen and Gilder*, 2006; *Elbra et al.*, 2007; *Kontny et al.*, 2007; *Louzada et al.*, 2008; *Raiskila et al.*, 2011; *Carporzen et al.*, 2012], reports of confirmed SRM in studied impact craters and extraterrestrial samples are rare to nonexistent. A key question is why SRM has not yet been conclusively identified. An important implication of this study is that SRM may not be readily observed in natural samples because of two factors: [1] SRM may be overprinted by other secondary remanences such as VRM, shock heating or metamorphic TVRM, IRM, or chemical remanent magnetization (CRM) from the creation of new ferromagnetic minerals during post-impact hydrothermal activity [*Quesnel et al.*, 2013], and [2] the acquisition efficiency of SRM may be too low for such a magnetization to be distinguishable from an underlying primary remanence (such as primary TRM) or a coexisting secondary remanence.

Regarding factor [1], the low coercivity nature of SRM means that it is highly susceptible to IRM overprinting by exposure to, for example, magnets or lightning strikes (e.g., *Carporzen et al.* [2012]). It is also possible that SRM is not often observed because the remanence may be at least partially eradicated by viscous relaxation over time. Although SRM is predominantly acquired by multidomain grains, prior observations indicate that single domain and multidomain rocks have similar susceptibilities to viscous acquisition and relaxation [*Dunlop*, 1983; *Yu and Tauxe*, 2006] while PSD grains are less susceptible to viscous effects [*Dunlop*, 1983]. Therefore, the persistence of PRM to unblocking temperatures approaching the Curie temperatures of the magnetic carriers suggests that at least some portion of an acquired SRM may be stable for billions of years according to the predictions of Néel theory [*Pullaiah et al.*, 1975; *Dunlop et al.*, 2000; *Weiss et al.*, 2000; *Garrick-Bethell and Weiss*, 2010]. In contrast, TVRM acquired from heating to a few hundred °C would likely eradicate much of any pre-existing SRM, given the prevalence of blocking and unblocking tails in PSD and MD samples. Secondary magnetizations at several impact craters have been attributed to shock-induced TVRM [*Jackson and Van der Voo*, 1986; *Iseri et al.*, 1989; *Schmidt and Williams*, 1991; *Elbra et al.*, 2007].

Regarding factor [2], $\alpha_{2\ \mathrm{mT}}$ was $\leq\sim10^{-2}$ (i.e., the 1.8 GPa PRM intensity was ≤1% of an equivalent-field TRM intensity) for 17 out of the 19 samples for which we determined PRM efficiencies. This means that a low-intensity SRM component may be difficult to identify if much stronger primary or other secondary remanences are present. However, when the paleofield strength range can be roughly estimated (like for terrestrial rocks), the disparity in the acquisition efficiencies of SRM and thermally activated forms of remanence such as VRM or TVRM provides an avenue with which to distinguish between them in natural samples by conducting paleointensity experiments. When conducting paleointensity experiments that assume a thermal origin of remanence in samples, thermally activated forms of remanence should yield paleointensities on order of the expected paleofield strength at the time of the impact. In contrast, SRM would yield paleointensities at minimum an order of magnitude weaker than the expected paleofield due to its low acquisition efficiency (at least for the ≤~2 GPa pressure range investigated in this study).

5. Conclusions

Our results indicate that an impact-related magnetization component may be attributable to (<2 GPa) SRM if (*i*) it can be efficiently cleaned via AF demagnetization, (*ii*) it persists to near-Curie unblocking temperatures during thermal demagnetization, and (*iii*) its inferred paleointensity (determined in a paleointensity experiment assuming a thermal origin of remanence) is significantly weaker than that of the magnetic field in which it was acquired (although the paleofield intensity is unlikely to be known a priori for extraterrestrial samples). However, the low acquisition efficiency and low coercivity nature of PRM relative to other forms of remanence may result in any record of SRM being obscured by other magnetization components. Furthermore, other impact-related processes such as hydrothermal alteration or shock heating may produce additional magnetizations that could overprint pre-existing SRM. Therefore, conclusive identification of SRM in natural samples would likely require studying rocks that have a fortuitous combination of relatively high PRM acquisition efficiencies (>~10% of TRM), minimal post-impact hydrothermal alteration, and low peak shock pressures (to preclude significant TVRM from shock heating). We are not currently aware of any unambiguous natural examples of such samples.

Acknowledgements

Data from this study is available upon request to the corresponding author. We thank the JSC staff and the Curation and Analysis Planning Team for Extraterrestrial Materials for allocating our lunar samples. We thank B. Carbone for administrative support. We thank two anonymous reviewers for their constructive comments. S. M. T., B. P. W., and C. S. thank the Brown-Massachusetts Institute of Technology (MIT) NASA Lunar Science Institute and Solar System Exploration Research Virtual Institute, the NASA Lunar Advanced Science and Exploration Program, and the NASA Solar System Workings Program.. B. P. W. and J. G. thank the MIT-France Seed Funds Program, the Projet International de Coopération Scientifique Program, and the People Programme (Marie Curie Actions) of the European Union under Research Executive Agency Grant 298355. B. P. W. thanks the Miller Institute for Basic Research in Science for support. N. L. S.-H. and J. G. thank the France-Berkeley Fund program. N. L. S.-H. and S. M. T. were supported by NSF Division of Earth Sciences Grant 1316395. S. M. T. was also supported by a Visiting Fellowship at the Institute for Rock Magnetism, University of Minnesota.

References Cited

Bogdanov, A., and A. Y. Vlasov (1966), On the effect of elastic stresses on the domain structure of magnetite, *Izv. Earth Physics*, *1*, 42-46.

Boyd, J. R., M. Fuller, and S. Halgedahl (1984), Domain wall nucleation as a controlling factor in the behaviour of fine magnetic particles in rocks, *Geophys. Res. Lett.,* 11, 193-196.

Carporzen, L., and S. A. Gilder (2006), Evidence for coeval late Triassic terrestrial impacts from the Rochechouart crater, *Geophys. Res. Lett.*, *33*, L19308.

Carporzen, L., B. P. Weiss, L. T. Elkins-Tanton, D. L. Shuster, D. S. Ebel, and J. Gattacceca (2011), Magnetic evidence for a partially differentiated carbonaceous chondrite parent body, *Proc. Natl. Acad. Sci. USA*, *108*, 6386-6389.

Carporzen, L., B. P. Weiss, S. Gilder, A. Pommier, and R. J. Hart (2012), Lightning remagnetization of the Vredefort impact crater: No evidence for impact-generated fields, *J. Geophys. Res.*, *117*(E01007), 1-17.

Chicot, D., J. Mendoza, A. Zaoui, G. Louis, V. Lepingle, F. Roudet, and J. Lesage (2011), Mechanical properties of magnetite (Fe3O4), hematite (α-Fe2O3) and goethite (α-FeO·OH) by instrumented indentation and molecular dynamics analysis, *Mater. Chem. Phys.*, *129*, 862-870.

Cisowski, S., M. Fuller, M. E. Rose, and P. J. Wasilewski (1973), Magnetic effects of experimental shocking of lunar soil, *Proc. Lunar Sci. Conf. 4th*, 3003-3017.

Cisowski, S., J. R. Dunn, M. Fuller, Y. Wu, M. F. Rose, and P. J. Wasilewski (1976), Magnetic effects of shock and their implications for lunar magnetism (II), *Proc. Lunar Sci. Conf. 7th*, 3299-3320.

Cournede, C., J. Gattacceca, M. Gounelle, P. Rochette, B. P. Weiss, and B. Zanda (2015), An early solar system magnetic field recorded in CM chondrites, *Earth Planet. Sci. Lett.*, *410*, 62-74.

Crawford, D. A., and P. H. Schultz (1993), The production and evolution of impact-generated magnetic fields, *Int. J. Impact Eng.*, *14*, 205-216.

Dunlop, D. J., M. Ozima, and H. Kinoshita (1969), Piezomagnetization of single-domain grains: A graphical approach, *J. Geomag. Geoelectr.*, *21*, 513-518.

Dunlop, D. J. (1983), Viscous magnetization of 0.04-100 μm magnetite, *Geophys. J. Roy. Astr. S.*, *74*, 667-687.

Dunlop, D. J., and O. Ozdemir (1997), *Rock Magnetism: Fundamentals and Frontiers*, 573 pp., Cambridge University Press, New York.

Dunlop, D. J., and O. Ozdemir (2000), Effect of grain size and domain state on thermal demagnetization tails, *Geophys. Res. Lett.*, *27*(9), 1311-1314.

Dunlop, D. J., O. Ozdemir, D. A. Clark, and P. W. Schmidt (2000), Time-temperature relations for the remagnetization of pyrrhotite (Fe7S8) and their use in estimating paleotemperatures, *Earth Planet. Sci. Lett.*, *176*, 107-116.

Dunlop, D. J., and O. Ozdemir (2001), Beyond Néel's theories: thermal demagnetization of narrow-band partial thermoremanent magnetizations, *Phys. Earth Planet. Inter.*, *126*, 43-57.

Elbra, T., A. Kontny, L. J. Pesonen, N. Schleifer, and C. Schell (2007), Petrophysical and paleomagnetic data of drill cores from the Bosumtwi impact structure, Ghana, *Meteorit. Planet Sci.*, *42*, 829-838.

Fu, R. R., B. P. Weiss, D. L. Shuster, J. Gattacceca, T. L. Grove, C. Suavet, E. A. Lima, L. Li, and A. T. Kuan (2012), An ancient core dynamo in Asteroid Vesta, *Science*, *338*, 238-241.

Fuller, M., and S. M. Cisowski (1987), Lunar paleomagnetism, *Geomagnetism*, *2*, 307-455.

Garrick, Bethell, I., and B. P. Weiss (2010), Kamacite blocking temperatures and applications to lunar magnetism, *Earth Planet. Sci. Lett.*, *294*, 1-7.

Gattacceca, J., and P. Rochette (2004), Toward a robust normalized magnetic paleointensity method applied to meteorites, *Earth Planet. Sci. Lett.*, *227*, 377-393.

Gattacceca, J., M. Boustie, B. P. Weiss, P. Rochette, E. A. Lima, L. E. Fong, and F. J. Baudenbacher (2006), Investigating impact demagnetization through laser impacts and SQUID microscopy, *Geology*, *34*(5), 333-336.

Gattacceca, J., A. Lamali, P. Rochette, M. Boustie, and L. Berthe (2007), The effects of explosive-driven shocks on the natural remanent magnetization and the magnetic properties of rocks, *Phys. Earth Planet. Inter.*, *162*, 85-98.

Gattacceca, J., L. Berthe, M. Boustie, F. Vadeboin, P. Rochette, and T. De Resseguier (2008), On the efficiency of shock magnetization processes, *Phys. Earth Planet. Inter.*, *166*, 1-10.

Gattacceca, J., M. Boustie, L. L. Hood, J.-P. Cuq-Lelandais, M. Fuller, N. S. Bezaeva, T. de Resseguier, and L. Berthe (2010a), Can the lunar crust be magnetized by shock: Experimental groundtruth, *Earth Planet. Sci. Lett.*, *299*, 42-53.

Gattacceca, J., M. Boustie, E. Lima, B. P. Weiss, T. de Resseguier, and J.-P. Cuq-Lelandais (2010b), Unraveling the simultaneous shock magnetization and demagnetization of rocks, *Phys. Earth Planet. Inter.*, *182*, 42-49.

Gattacceca, J., et al. (2013), Opaque minerals, magnetic properties, and paleomagnetism of the Tissint meteorite, *Meteorit. Planet Sci.*, doi:http://dx.doi.org/10.1111/maps.12172.

Gilder, S., and M. Le Goff (2008), Systematic pressure enhancement of titanomagnetite magnetization, *Geophys. Res. Lett.*, *35*, L10302.

Gilder, S. A., R. Egli, R. Hochleitner, S. C. Roud, M. W. R. Volk, M. Le Goff, and M. de Wit (2011), Anatomy of a pressure-induced, ferromagnetic-to-paramagnetic transition in pyrrhotite: Implications for the formation pressure of diamonds, *J. Geophys. Res.*, *116*, doi:10:1029/2011JB008292.

Halekas, J. S., D. L. Mitchell, R. P. Lin, L. L. Hood, M. H. Acuna, and A. B. Binder (2002), Demagnetization signatures of lunar impact craters, *Geophys. Res. Lett.*, *29*, doi:10.1029/2001GL013924.

Halls, H. C. (1979), The Slate Islands meteorite impact site: a study of shock remanent magnetization., *Geophys. J. Roy. Astr. S.*, *59*, 553-591.

Hodych, J. P. (1977), Single-domain theory for the reversible effect of small uniaxial stress upon the remanent magnetization of rock, *Can. J. Earth Sci.*, *14*, 2047-2061.

Hood, L. L., N. C. Richmond, E. Pierazzo, and P. Rochette (2003), Distribution of crustal magnetic fields on Mars: shock effects of basin-forming impacts, *Geophys. Res. Lett.*, *30*, 1281, doi:10.1029/2002GL016657.

Hood, L. L., and N. A. Artemieva (2008), Antipodal effects of lunar basin-forming impacts: Initial 3D simulations and comparisons with observations, *Icarus*, *193*, 485-502.

Iseri, D. A., J. W. Geissman, H. E. Newsom, and G. Graup (1989), Paleomagnetic and rock magnetic examination of the natural remanent magnetization of suevite deposite at Ries crater, West Germany, *Meteoritics*, *24*, 280.

Jackson, M., and R. Van der Voo (1986a), A paleomagentic estimate of the age and thermal history of the Kentland, Indiana cryptoexplosion structure, *J. Geol.*, *94*, 713-723.

Kirschvink, J., R. Kopp, T. Raub, C. Baumgartner, and J. Holt (2008), Rapid, precise, and high-sensitivity acquisition of paleomagnetic and rock magnetic data: Development of a low-noise automatic sample changing system for superconducting rock magnetometers, *Geochem. Geophy. Geosy.*, *9*(5), 1-18.

Kletetschka, G., T. Kohout, and P. Wasilewski (2003), Magnetic remanence in the Murchison meteorite, *Meteorit. Planet Sci.*, *38*, 399.

Kontny, A., T. Elbra, J. Just, L. J. Pesonen, A. M. Schleicher, and J. Zolk (2007), Petrography and shock-related remagnetization of pyrrhotite in drill cores from the Bosumtwi Impact Crater Drilling Project, Ghana, *Meteorit. Planet Sci.*, *42*, 811-827.

Ledbetter, H. M., and R. P. Reed (1973), Elastic properties of metals and alloys, I. Iron, nickel, and iron-nickel alloys, *J. Phys. Chem. Ref. Data*, *2*, 531-617.

Louzada, K. L., S. T. Stewart, and B. P. Weiss (2007), Effect of shock on the magnetic properties of pyrrhotite, the Martian crust, and meteorites, *Geophys. Res. Lett.*, *34*, L05204, doi:10.1029/2006GL027685.

Louzada, K. L., B. P. Weiss, A. C. Maloof, S. T. Stewart, N. Swanson-Hysell, and S. A. Soule (2008), Paleomagnetism of Lonar Impact Crater, India, *Earth Planet. Sci. Lett.*, *275*, 309-319.

Louzada, K. L., and S. T. Stewart (2009), Effects of planet curvature and crust on the shock pressure field around impact basins, *Geophys. Res. Lett.*, *36*, L15203, doi:10.1029/2009GL037869.

Louzada, K. L., S. T. Stewart, B. P. Weiss, J. Gattacceca, and N. S. Bezaeva (2010), Shock and static pressure demagnetization of pyrrhotite and implications for the Martian crust, *Earth Planet. Sci. Lett.*, *290*, 90-101.

Mang, C., A. Kontny, J. Fritz, and R. Schneider (2013), Shock experiments up to 30 GPa and their consequences on microstructures and magnetic properties in pyrrhotite, *Geochem. Geophy. Geosy.*, *14*(1), 64-85, doi:10.1029/2012GC004242.

Martin, R. J., and J. S. Noel (1988), The influence of stress path on thermoremanent magnetization, *Geophys. Res. Lett.*, *15*, 507-510.

Muxworthy, A. R., and W. Williams (2006), Observations of viscous magnetization in multidomain magnetite, J. Geophys. Res., *111*, B01103, doi:10.1029/2005JB003902.

Nagata, T. (1966), Main characteristics of piezo-magnetization and their qualitative interpretation, *J. Geomag. Geoelectr.*, *18*, 81-97.

Nagata, T., and Kinoshita, H. (1967), Effect of hydrostatic pressure on magnetostriction and magnetocrystalline anisotropy of magnetite, *Phys. Earth Planet. Inter.*, 1, 44-48.

Nagata, T., and B. J. Carleton (1968), Notes on piezo-remanent magnetization of igneous rocks, *J. Geomag. Geoelectr.*, *20*(3), 115-127.

Nagata, T. (1970), Anisotropic magnetic susceptibility of rocks under mechanical stresses, *Pure Appl. Geophys.*, *78*(1), 110-122.

Nagata, T. (1971), Introductory notes on shock remanent magnetization and shock demagnetization of igneous rocks, *Pure Appl. Geophys.*, *89*, 159-177.

Nagata, T. (1973), Piezo-remanent magnetization of lunar rocks, *Pure Appl. Geophys.*, *110*, 2022-2030.

Néel, L. (1955), Some theoretical aspects of rock magnetism, *Adv. Phys.*, *12*, 191-242.

Pesonen, L. J., S. Elo, M. Lehtinen, T. Jokinen, R. Puranen, and L. Kivekas (1999), Lake Karikkoselka impact structure, central Finland: New geophysical and petrographic results., *Geol. S. Am. S.*, *339*, 131-147.

Pohl, J., U. Bleil, and U. Hornemann (1975), Shock magnetization and demagnetization of basalt by transient stress up to 10 kbar., *J. Geophys.*, *41*, 23-41.

Pullaiah, G., E. Irving, K. L. Buchan, and D. J. Dunlop (1975), Magnetization changes caused by burial and uplift, *Earth Planet. Sci. Lett.*, *28*, 133-143.

Quesnel, Y., J. Gattacceca, G. R. Osinski, and P. Rochette (2013), Origin of the central magnetic anomaly at the Haughton impact structure, Canada, *Earth Planet. Sci. Lett.*, *367*, 116-122.

Raiskila, S., J. Salminen, T. Elbra, and L. J. Pesonen (2011), Rock magnetic and paleomagnetic study of the Keurusselka impact structure, central Finland, *Meteorit. Planet Sci.*, *46*, 1670-1687.

Robertson, P. B., and R. A. Grieve (1977), Shock attenuation at terrestrial impact structures, in *Impact and Explosion Cratering*, edited by D. J. Roddy, R. O. Pepin and R. B. Merrill, pp. 687-702, Pergamon Press, New York.

Robertson, W. A. (1967), Manicouagan, Quebec, paleomagnetic results, *Can. J. Earth Sci.*, *4*, 641-649.

Rochette, P., J. Gattacceca, L. Bonal, M. Bourot-Denise, V. Chevrier, J.-P. Clerc, G. Consolmagno, L. Folco, M. Gounelle, T. Kohout, L. Pesonen, E. Quirico, L. Sagnotti, and A. Skripnik (2008), Magnetic classification of stony meteorites: 2. Non-ordinary chondrites, *Meteorit. Planet. Sci.*, *43*, 959-980.

Sadykov, R. A. (2008), Nonmagnetic high pressure cell for magnetic remanence measurements up to 1.5 GPa in a superconducting quantum interference device magnetometer, *Rev. Sci. Instrum.*, *79*(11), 115102.

Schmidt, P. W., and G. E. Williams (1991), Paleomagnetic correlation of the Acraman impact structure and the Late Proterozoic Bunyeroo ejecta horizon, South Australia, *Aust. J. Earth Sci.*, *38*, 283-289.

Shea, E. K., B. P. Weiss, W. S. Cassata, D. L. Shuster, S. M. Tikoo, J. Gattacceca, T. L. Grove, and M. D. Fuller (2012), A long-lived lunar core dynamo, *Science*, *335*, 453-456.

Srnka, L. J. (1977), Spontaneous magnetic field generation in hypervelocity impacts, *Proc. Lunar Planet. Sci. Conf. 8th* 785-792.

Stewart, S. T., A. Seifter, G. B. Kennedy, M. R. Furlanetto, and A. W. Obst (2007), Measurements of emission temperatures from shocked basalt: hot spots in meteorites, *Proc. Lunar Planet. Sci. 38th*, 2413.

Stoffler, D., G. Ryder, B. A. Ivanov, N. A. Artemieva, M. J. Cintala, and R. A. F. Grieve (2006), Cratering history and lunar chronology, *Rev. Mineral. Geochem.*, *60*, 519-596.

Suavet, C., B. P. Weiss, W. S. Cassata, D. L. Shuster, J. Gattacceca, L. Chan, I. Garrick-Bethell, J. W. Head, T. L. Grove, and M. D. Fuller (2013), Persistence and origin of the lunar core dynamo, *Proc. Natl. Acad. Sci. USA*, *110*(21), 8453-8458, doi:10.1073/pnas.1300341110.

Suavet, C., B. P. Weiss, and T. L. Grove (2014), Controlled-atmosphere thermal demagnetization and paleointensity analyses of extraterrestrial rocks, *Geochem. Geophy. Geosy.*, *15*(7), 2733-2743.

Swanson-Hysell, N. L., A. A. Vaughan, M. R. Mustain, and K. E. Asp (2014), Confirmation of progressive plate motion during the Midcontinent Rift’s early magmatic stage from the Osler Volcanic Group, Ontario, Canada, *Geochem. Geophys. Geosyst.*, 15, 2039– 2047.

Swartzendruber, L. J., V. P. Itkin, and C. B. Alcock (1991), The Fe-Ni (iron-nickel) system, *J. Phase Equil.*, *12*, 288-312.

Tikoo, S. M., B. P. Weiss, J. Buz, E. A. Lima, E. K. Shea, G. Melo, and T. L. Grove (2012), Magnetic fidelity of lunar samples and implications for an ancient core dynamo, *Earth Planet. Sci. Lett.*, *337-338*, 93-103.

Tikoo, S. M., B. P. Weiss, W. Cassata, D. L. Shuster, J. Gattacceca, E. A. Lima, C. Suavet, F. Nimmo, and M. Fuller (2014), Decline of the lunar core dynamo, *Earth Planet. Sci. Lett.*, *404*, 89-97.

Wasilewski, P. (1981), New magnetic results from Allende C3 (V), *Phys, Earth Planet. Inter.*, *26*, 134-148.

Weiss, B. P., J. L. Kirschvink, F. J. Baudenbacher, H. Vali, N. T. Peters, F. A. MacDonald, and J. P. Wikswo (2000), A low temperature transfer of ALH84001 from Mars to Earth, *Science*, *290*, 791-795.

Weiss, B. P., J. Gattacceca, S. Stanley, P. Rochette, and U. R. Christensen (2010), Paleomagnetic records of meteorites and early planetesimal differentiation, *Space Sci. Rev.*, *152*, 341-390.

Weiss, B. P., and S. M. Tikoo (2014), The lunar dynamo, *Science*, *246*, doi:10.1126/science.1246753.

Xu, S., and D. J. Dunlop (1994), Theory of partial thermoremanent magnetization in multidomain grains 2. Effect of microcoercivity distribution and comparison with experiment, *J. Geophys. Res.*, *99*(B5), 9025-9033.

Yu, Y., and L. Tauxe (2006), Acquisition of viscous remanent magnetization, *Phys. Earth Planet. Inter.*, *159*, 32-42.

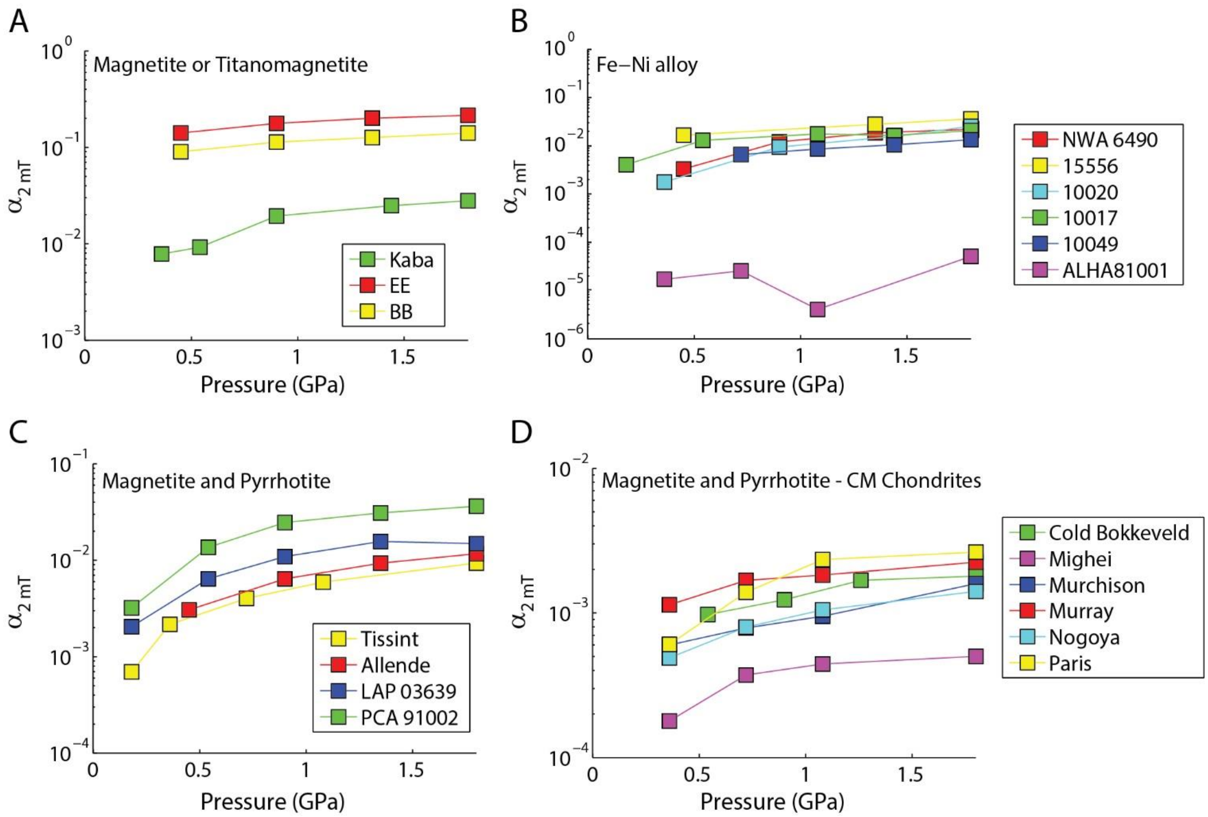

Fig. 1. PRM efficiency relative to TRM at AF 2 mT ($\alpha_{2\ mT}$) at pressures ranging up to 1.8 GPa for samples of various magnetic mineralogies. (A) Samples with magnetite and titanomagnetite. (B) Samples with Fe-Ni alloy. (C) Samples with pyrrhotite alone or a mixture of magnetite and pyrrhotite. (D) CM chondrite samples with magnetite and pyrrhotite.

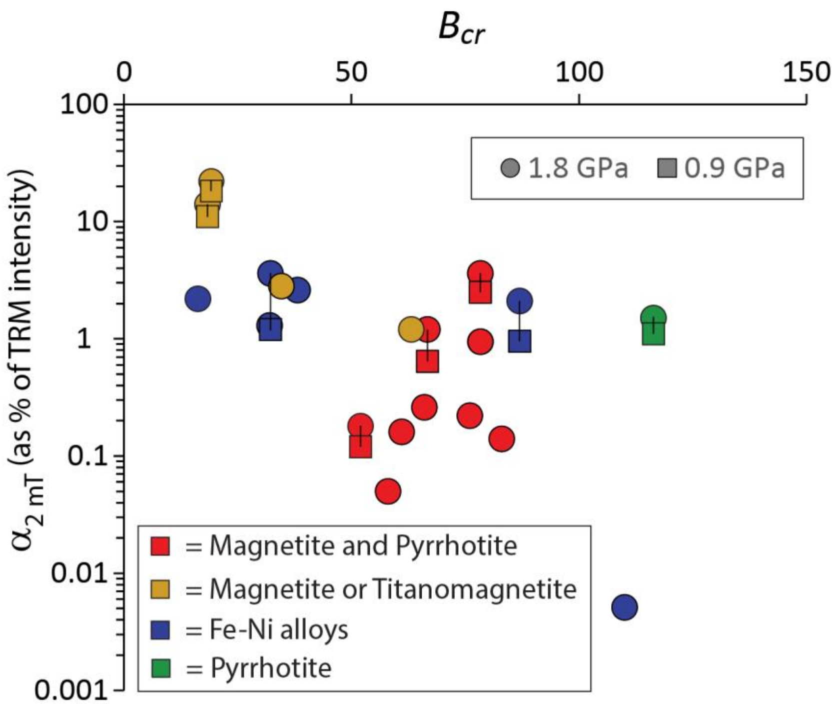

Fig.2. PRM efficiency versus remanent coercivity. The ordinate gives the PRM efficiency relative to TRM at an AF level of 2 mT ($\alpha_{2\ mT}$), expressed here as a percentage of the intensity of TRM acquired in an equivalent ambient field, for PRM applied at 1.8 GPa (dark gray circles) and 0.9 GPa (light gray squares). The abscissa gives the remanent coercivity (B_{cr}). PRM data collected from the same subsamples at different pressures are joined by lines.

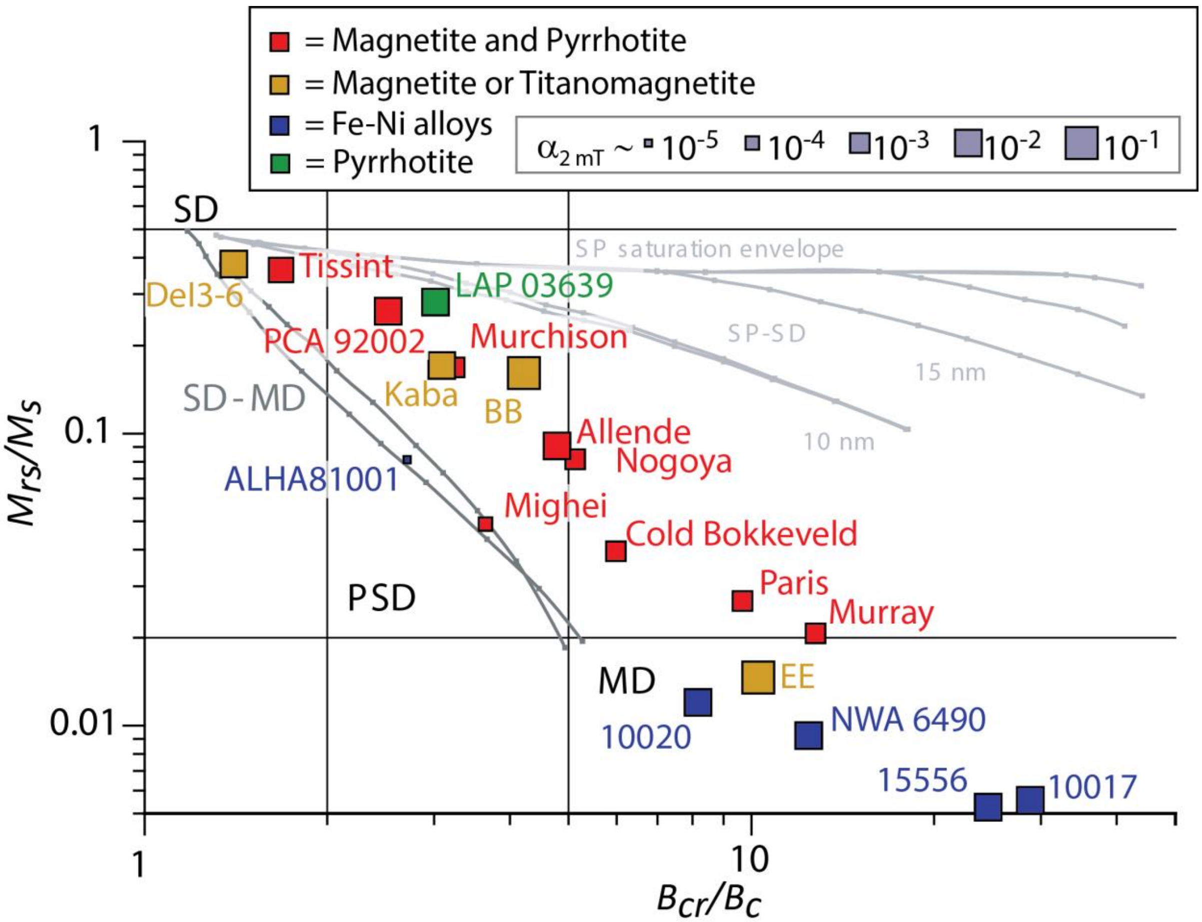

Fig. 3. Dunlop-Day plot of hysteresis parameters. The ordinate gives the magnitude of the saturation remanent magnetization (M_{rs}) divided by the magnitude of the saturation magnetization (M_s). The abscissa gives the remanent coercivity (B_{cr}) divided by the coercive force (B_c). Squares denote sample positions. Red symbols denote samples with a combination of magnetite and pyrrhotite ferromagnetic mineralogies. Yellow symbols denote samples with magnetite or titanomagnetite. Blue symbols denote samples with Fe-Ni alloys. Green symbols denote samples with pyrrhotite. Symbol sizes are scaled according to their PRM efficiency ($\alpha_{2\ \mathrm{mT}}$). Straight black vertical and horizontal lines divide the plot into rectangular regions representing single domain (SD), pseudo-single domain (PSD), and multidomain (MD) regimes.

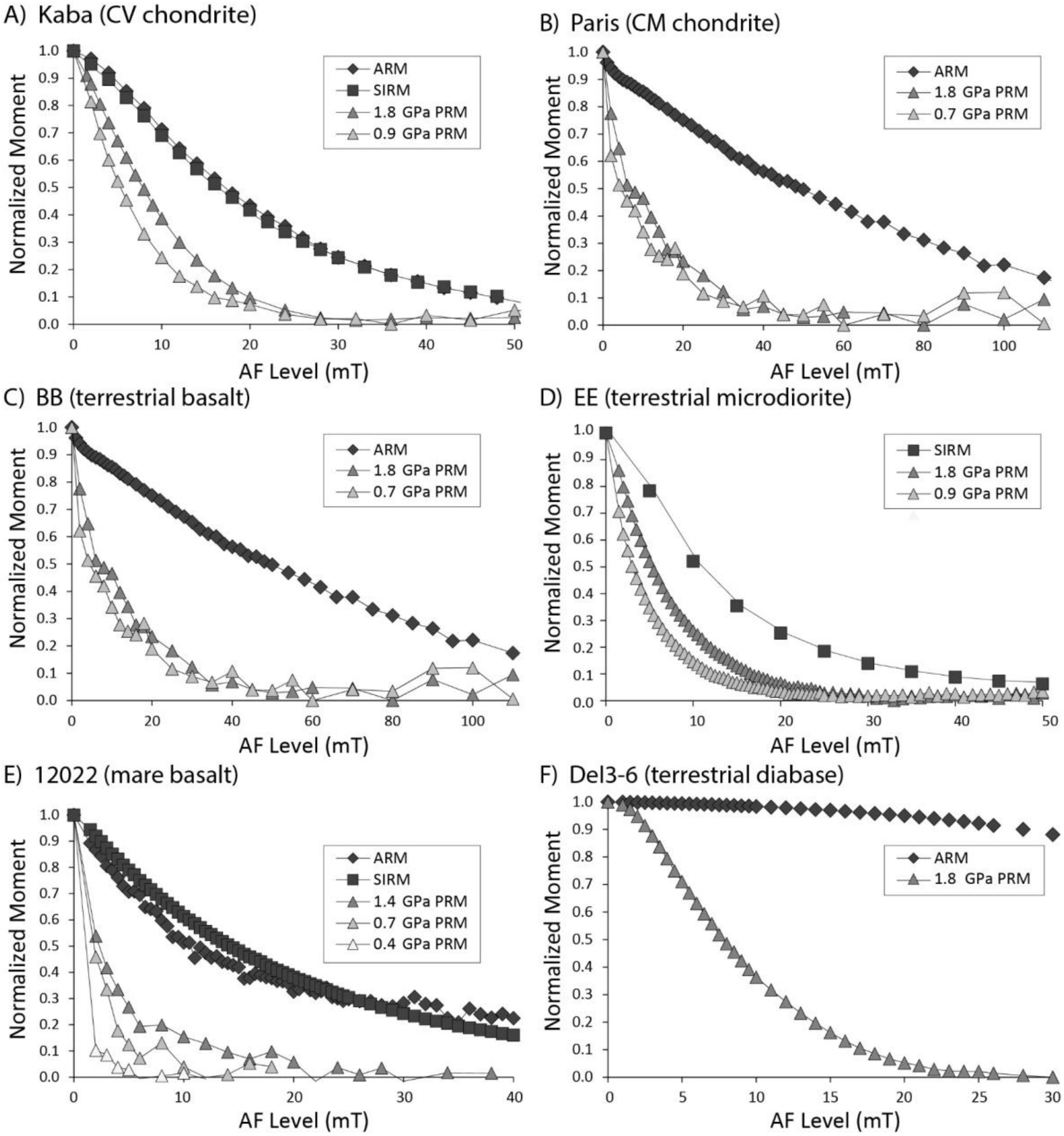

Fig. 4. AF demagnetization of PRM (triangles), TRM (circles), ARM (diamonds), and/or SIRM (squares). The ordinate shows the normalized magnetic moment and the abscissa shows the corresponding AF level. Shown samples (magnetic mineralogies) include: (**A**) CV3 chondrite Kaba (magnetite), (**B**) CM chondrite Paris (magnetite and pyrrhotite), (**C**) terrestrial basalt BB (titanomagnetite), (**D**) terrestrial microdiorite EE (magnetite), (**E**) mare basalt 12022 (FeNi), and (**F**) terrestrial diabase DeI3-6 (magnetite).

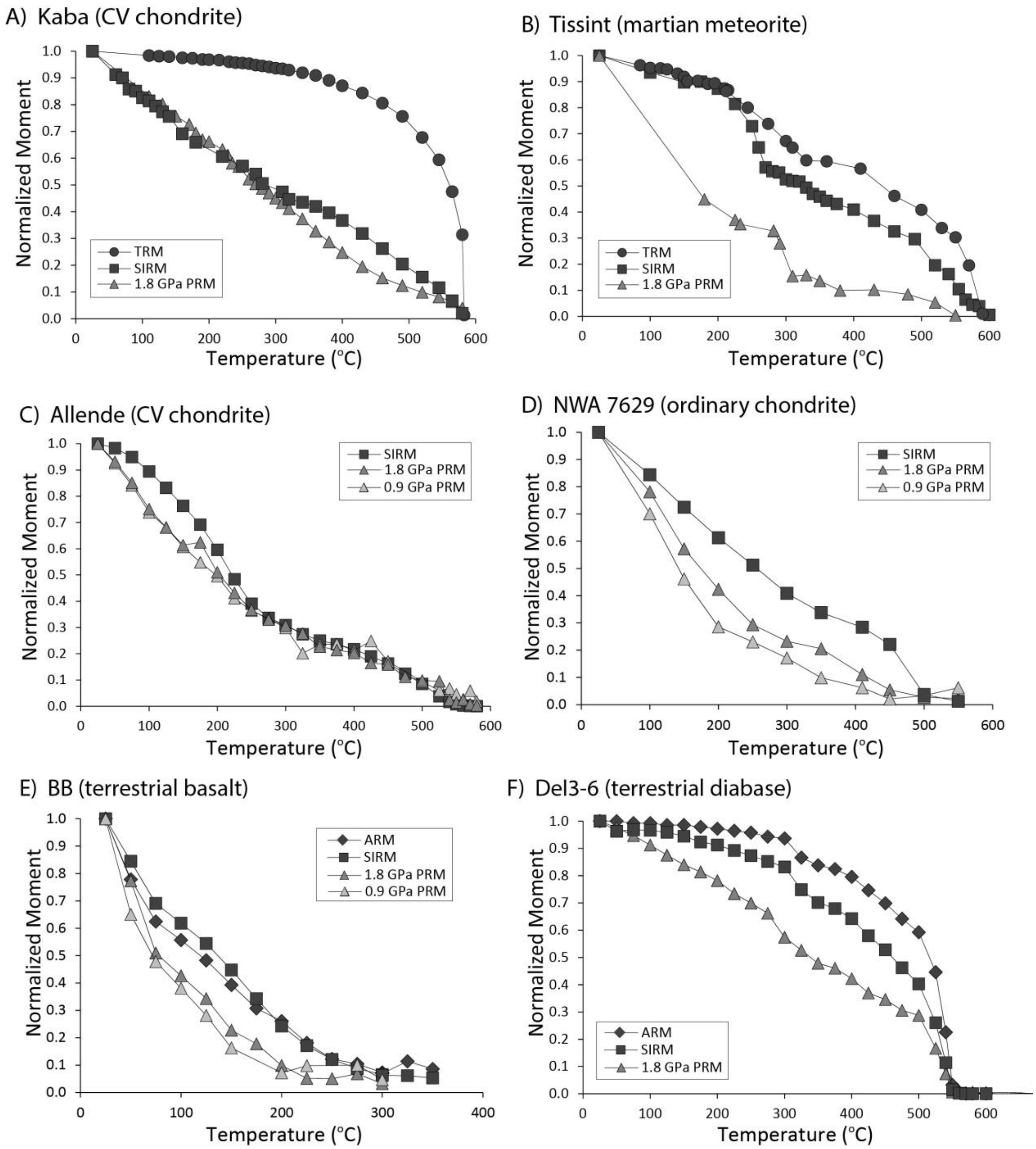

Fig. 5. Thermal demagnetization of PRM (triangles), TRM (circles), ARM (diamonds), and/or SIRM (squares). The ordinate shows the normalized magnetic moment and the abscissa shows the corresponding temperature step. Shown samples (magnetic mineralogies) include: (**A**) CV3 chondrite Kaba (magnetite), (**B**) Martian meteorite Tissint (magnetite and pyrrhotite), (**C**) CV3 chondrite Allende (magnetite and pyrrhotite), (**D**) NWA 7629 (FeNi). (**E**) basalt BB (titanomagnetite), and (**F**) diabase DeI3-6 (titanomagnetite).

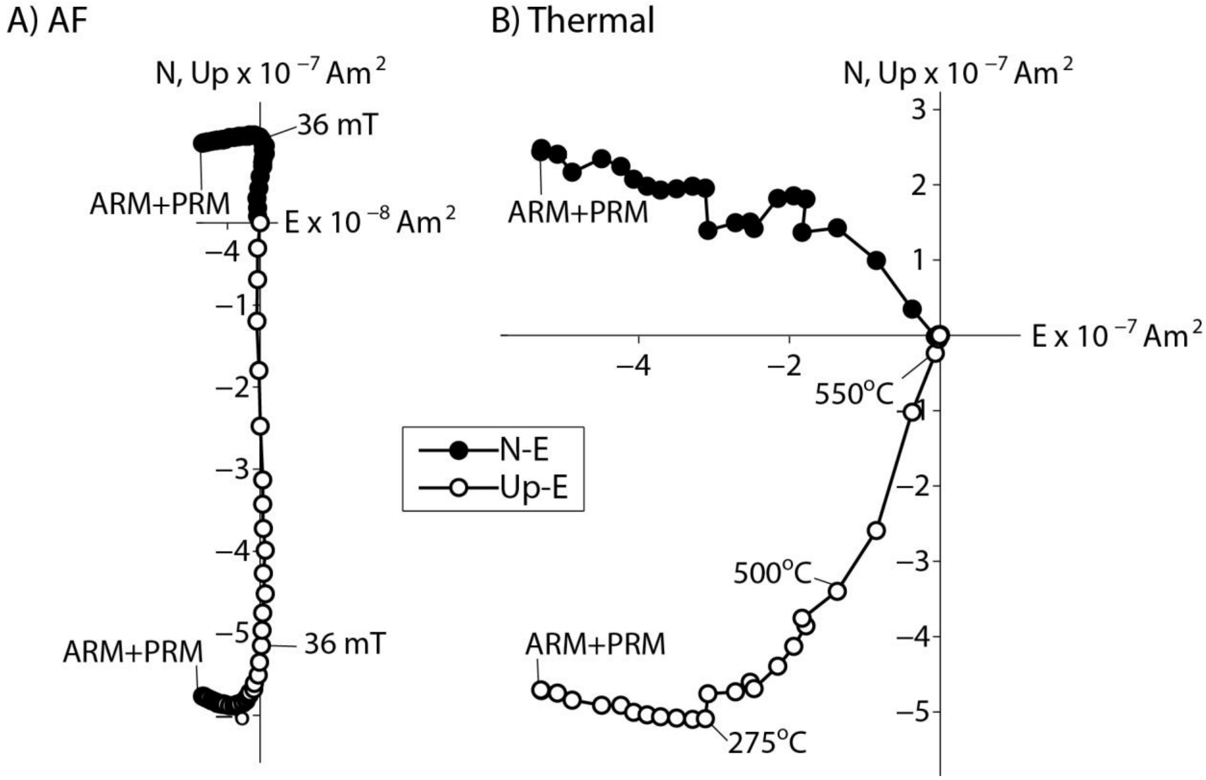

Fig. 6. Demagnetization of ARM with an overlying, orthogonally applied, PRM for two subsamples of terrestrial diabase sample DeI3-6. (**A**) AF demagnetization. (**B**) thermal demagnetization. Open and closed circles represent projections of the NRM vector onto the vertical (Z-E) and horizontal planes (N-E), respectively. Selected AF amplitude and temperature steps are labeled. PRMs were imparted using a 500 µT dc field at 1.8 GPa peak pressure while ARMs were imparted using a 100 µT dc field in a peak ac field of 300 mT. Disparities in remanence intensities between the two subsamples may be attributed to differences in sample mass and vector subtraction of a spurious gyroremanent magnetization component at the end of the AF demagnetization experiment in part (A).

Table 1. Magnetic and petrophysical properties of samples.

Sample Name	Magnetic carrier	M_{rs} (Am²/kg)	M_s (Am²/kg)	M_{rs}/M_s	B_{cr} (mT)	B_c (mT)	B_{cr}/B_c	$\alpha_{2\ mT}$ *(1.8 GPa)*	$\alpha_{2\ mT}$ *(0.9 GPa)*	Reference
NWA 7629 (H5 chondrite, W1)	Fe-Ni alloy	5.3×10^{-2}	4.52	1.2×10^{-1}	31	2.5	12.4		-	this study
NWA 6490 (L5 chondrite, W1)	Fe-Ni alloy	3.3×10^{-1}	31.3	9.2×10^{-3}	16	1.3	12.5	2.2×10^{-2}	-	this study
15556 (lunar mare basalt)	Fe-Ni alloy	6.1×10^{-4}	0.10	5.2×10^{-3}	32	1.3	24.8	3.6×10^{-2}	1.2×10^{-2}	Tikoo et al. (2012)
12022 (lunar mare basalt)	Fe-Ni alloy	8.8×10^{-4}	0.08	1.2×10^{-2}	49	2.0	22.2	-	-	Tikoo et al. (2014)
10020 (lunar mare basalt)	Fe-Ni alloy	1.5×10^{-3}	0.01	1.2×10^{-2}	38	4.7	8.2	2.6×10^{-2}	-	Shea et al. (2012)
10017 (lunar mare basalt)	Fe-Ni alloy	9.4×10^{-4}	0.17	5.5×10^{-3}	87	3.0	29.0	2.1×10^{-2}	9.5×10^{-3}	Suavet et al. (2013)
10049 (lunar mare basalt)	Fe-Ni alloy	1.2×10^{-3}	-	-	32	-	-	1.3×10^{-2}	-	Suavet et al. (2013)
ALHA81001 (eucrite)	Fe-Ni alloy	3.9×10^{-4}	0.01	8.1×10^{-2}	110	41.0	2.7	5.1×10^{-5}	-	Fu et al. (2012)
Allende (CV3 chondrite)	Pyrrhotite, Magnetite	5.9×10^{-2}	0.66	9.0×10^{-2}	67	13.8	4.8	1.2×10^{-2}	6.4×10^{-3}	Wasilewski (1981)
Kaba (CV3 chondrite)	Magnetite	1.8×10^{0}	10.5	1.7×10^{-1}	35	14.5	2.4	2.8×10^{-2}	-	this study
BB (terrestrial basalt)	Titanomagnetite	9.8×10^{-2}	0.62	1.6×10^{-1}	18	5.2	3.5	1.4×10^{-1}	1.1×10^{-1}	Gattacceca et al. (2007)
Del3-6 (terrestrial diabase)	Magnetite	8.0×10^{-1}	2.13	3.8×10^{-1}	63	44.4	1.4	1.2×10^{-2}	-	this study
EE (terrestrial microdiorite)	Magnetite	2.4×10^{-2}	0.14	1.9×10^{-1}	19	1.9	10.3	2.2×10^{-1}	1.8×10^{-1}	Gattacceca et al. (2007)
LAP 03639 (R chondrite)	Pyrrhotite	1.6×10^{-2}	0.06	2.8×10^{-1}	116	38.9	3.0	1.5×10^{-2}	1.1×10^{-2}	this study
PCA 91002 (R chondrite)	Pyrrhotite, Magnetite	2.5×10^{-2}	0.10	2.5×10^{-1}	78	32.6	2.4	3.6×10^{-2}	2.5×10^{-2}	this study
Cold Bokkeveld (CM chondrite)	Pyrrhotite, Magnetite	6.1×10^{-2}	1.53	4.0×10^{-2}	52	10.0	5.4	1.8×10^{-3}	1.2×10^{-3}	Cournede et al. (2015)
Mighei (CM chondrite)	Pyrrhotite, Magnetite	3.6×10^{-2}	0.71	5.0×10^{-2}	58	19.0	3.0	5.0×10^{-4}	-	Cournede et al. (2015)
Murchison (CM chondrite)	Pyrrhotite, Magnetite	8.9×10^{-2}	0.52	1.7×10^{-1}	61	23.0	2.6	1.6×10^{-3}	-	Cournede et al. (2015)
Murray (CM chondrite)	Pyrrhotite, Magnetite	1.2×10^{-1}	5.69	2.1×10^{-2}	76	6.0	13.4	2.2×10^{-3}	-	Cournede et al. (2015)
Nogoya (CM chondrite)	Pyrrhotite, Magnetite	8.7×10^{-2}	1.05	8.3×10^{-2}	83	18.0	4.5	1.4×10^{-3}	-	Cournede et al. (2015)
Paris (CM chondrite)	Pyrrhotite, Magnetite	1.2×10^{-1}	4.60	2.7×10^{-2}	66	7.0	9.6	2.6×10^{-3}	-	Cournede et al. (2015)
Tissint (shergottite)	Pyrrhotite, Magnetite	6.2×10^{-2}	0.17	3.6×10^{-1}	78	46.4	1.7	9.4×10^{-3}	-	Gattacceca et al. (2013)

Note: The first column contains the sample name and description. The second column contains the dominant magnetic mineralogy. The third and fourth columns contain the saturation remanent magnetization (M_{rs}) and saturation magnetization (M_s), respectively. The fifth column contains M_{rs}/M_s. The sixth and seventh columns contain the remanent coercivity (B_{cr}) and coercivity (B_c) respectively. The eighth column contains B_{cr}/B_c. The ninth and tenth columns contain efficiency of 1.8 GPa and 0.9 GPa PRM relative to TRM, respectively. SIRM normalization was used to obtain TRM estimates for all the PRM efficiency calculations. The eleventh column contains the sources for ferromagnetic mineralogy descriptions and hysteresis parameters.